Shears mechanism and development of collectivity in ^{141}Sm

S. Rajbanshi,[1,2] Sajad Ali,[1] Abhijit Bisoi,[3] Somnath Nag,[4] S. Saha,[5] J. Sethi,[5] T. Bhattacharjee,[6] S. Bhattacharyya,[6]
S. Chattopadhyay,[1] G. Gangopadhyay,[7] G. Mukherjee,[6] R. Palit,[5] R. Raut,[8] M. Saha Sarkar,[1] A. K. Singh,[9]
T. Trivedi,[10] and A. Goswami[1,*]

[1]*Saha Institute of Nuclear Physics, Kolkata 700064, India*
[2]*Dum Dum Motijheel College, Kolkata 700074, India*
[3]*Indian Institute of Engineering Science and Technology, Howrah 711103, India*
[4]*National Institute of Technology, Raipur 492010, India*
[5]*Tata Institute of Fundamental Research, Mumbai 400005, India*
[6]*Variable Energy Cyclotron Center, Kolkata 700064, India*
[7]*Department of Physics, University of Calcutta, Kolkata 700009, India*
[8]*UGC-DAE-Consortium for Scientific Research, Kolkata 700098, India*
[9]*Indian Institute of Technology, Kharagpur 721302, India*
[10]*Guru Ghasidas Vishayavidyalaya, Bilaspur 495009, India*

High-spin states in the dipole structure of ^{141}Sm have been investigated using the fusion-evaporation reaction
^{116}Cd (^{31}P,$p5n$) at beam energy 148 MeV using the Indian National Gamma Array. The spin parity of the
observed dipole bands I and II has been established firmly from the spectroscopic measurements. Level lifetimes
of several levels in the dipole bands I and II have been measured using the Doppler shift attenuation method. The
smooth decrease of the $B(M1)$ values with spin exhibits a clear signature of the magnetic rotational character of
the dipole band I. Comparisons between the experimental characteristics and the semiclassical shears mechanism
with the principal axis cranking model calculation show that the dipole band I may be interpreted as a magnetic
rotational band.

I. INTRODUCTION

Magnetic rotation phenomenon, observed more than a
decade ago, represents a mechanism for generation of angular
momentum in nuclei that are almost spherical or weakly
deformed. It leads to rotationlike bands consisting of strong
intraband magnetic dipole ($M1$) transitions, whereas the
crossover electric quadrupole ($E2$) transitions are either weak
or almost absent, indicating that they do not originate from the
usual rotational motion of a deformed system. These bandlike
structures have been designated as the magnetic rotational
(MR) bands [1]. Collective rotations in a finite many-body
system such as the nucleus are only possible for configurations
with a well-defined orientation and small fluctuations around
it, i.e., with a strong violation of symmetry in the intrinsic
frame [2,3], leading to enhanced $E2$ transitions. Magnetic
rotation occurs in systems with small deformation of the
density distribution and therefore the symmetry violation is
possible only by the current distribution of the valence neutron
and proton quasiparticles, leading to strong $M1$ transitions [4].
The detailed discussion on the shears mechanism was reported
in an extensive review article by Clark and Macchiavelli [1].

The MR bands have been observed in weakly deformed
nuclei across the nuclear chart in different mass regions
with $A \approx 80$, 100, 140, and 190 [5–8]. The findings have
been extensively reviewed by a number of authors such as
by Hübel [9] and Amita *et al.* [10]. These nuclei satisfy

the requisite conditions for the MR phenomenon, such as
near-spherical shape, availability of high j orbitals, and
ability to generate angular momentum through the particle
and hole excitations in the neutron and proton sectors [4].
Theoretical interpretation of the MR phenomenon has been
proposed within the framework of the tilted axis cranking
(TAC) [11,12] and the shears mechanism with principal axis
cranking (SPAC) [13–15] models. In the latter description,
the states along a MR band are perceived to be generated
by the gradual alignment of the angular momentum vectors,
produced by the valence particles and holes. This mechanism
provides a large transverse component of the magnetic dipole
moment ($\mu_\perp$) which decreases with spin. As a result, the
$B(M1)$ values of the states also decrease with spin along the
band [$B(M1) \propto \mu_\perp^2$]. Indeed, among several observed features
of the MR phenomenon, the most stringent experimental
signature is the decreasing behavior of the $B(M1)$ value with
increasing rotational frequency (ω) along the band.

The behavior of the dipole bands observed in different
mass regions has evoked interpretation in terms of shell-model
calculations and its interaction with the collective degrees of
freedom. As an example, the characteristics observed for the
dipole bands in ^{82,84}Rb isotopes were well described in the
TAC model on the basis of four-quasiparticle configuration
[5]. The calculation reproduced the bandlike properties and
the experimental transition probabilities for both the nuclei.
However, the excited states and the transitions strengths for
^{84}Rb were also reproduced in a shell-model calculation,
though the detailed properties of the MR band cannot be
described because of the limited configuration space. This

*asimananda.goswami@saha.ac.in

alternative description of the MR band in terms of the shell-model picture raises an important question on the coexistence of different excitation modes in this mass region. In fact, it was pointed out [16] that the observation of MR bands is expected in a very narrow region of mass number around $A \sim 80$. This is because a small change in the proton and neutron numbers led to a large change of nuclear deformation in this mass region owing to the change in the occupation of the intruder high-j $g_{9/2}$ orbital. Thus, the nuclear deformation played a very crucial role in the generation of angular momentum through the shears mechanism.

This question was specifically addressed to study the observed dipole bands in ^{124}Xe [17] and ^{128}Ba [18] nuclei. In both cases the dipole bands were interpreted as high-K prolate bands rather than as oblate shear bands [19]. Thus, the possible way for the generation of angular momentum through the shears mechanism depends very critically on the motion owing to deformed collective degrees of freedom and its interaction with the single-particle states.

While MR phenomena have been primarily observed in weakly deformed systems, it is interesting to consider the evolution of deformation characteristics along such bands. There has been precedent for changing deformation as well as increasing collectivity with spin in the MR band observed in, for instance, ^{139}Sm nucleus [20]. A probe for similar observations in other nuclei exhibiting shears structure is warranted.

The present paper reports the quest for the MR phenomenon in the ^{141}Sm nucleus. Previously, the high-spin states in ^{141}Sm have been studied by Lach *et al.* [21] and Cardona *et al.* [22] using the ^{142}Nd($\alpha, 5n$) and ^{116}Cd(^{29}Si$, 4n$) reactions, respectively. Both these studies have reported a dipole band with bandhead spin of 25/2 at excitation energy of 3.3 MeV. However, Cardona *et al.* [22] proposed the dipole structure with no parity assignments while parity assignments of these levels up to the $I^{\pi} = 33/2^{-}$ have been reported by Lach *et al.* [21]. In the present work, the dipole structure in ^{141}Sm has been reinvestigated and has been rearranged as spectacle of the two dipole bands I and II. The spin-parity of the states in the dipole bands I and II have been confirmed from the spectroscopic measurements. Lifetimes of the states in the dipole bands I and II have been determined using the Doppler shift attenuation method (DSAM) technique. The primary objective of the present work was to establish the MR phenomenon in the ^{141}Sm nucleus through investigation of the $B(M1)$ values in the aforementioned dipole bands and theoretical interpretation of the same using the SPAC model.

II. EXPERIMENTAL DETAILS AND DATA ANALYSIS

High-spin states in ^{141}Sm were populated using the heavy-ion fusion-evaporation reaction ^{116}Cd(^{31}P$, p5n$) at the beam energy 148 MeV. The ^{31}P beam was provided by the Pelletron Linac Facility at Tata Institute of Fundamental Research (TIFR), Mumbai, India. The target was 99% enriched 2.4 mg/cm^2 of ^{116}Cd on a 14.5 mg/cm^2 thick backing of Pb. The recoil velocity of the compound nucleus was $\approx$2% of c. The deexciting γ-ray transitions were detected by the Indian National Gamma Array (INGA) [23,24], which consisted of 19 Compton-suppressed clover detectors arranged in six different

angles [90°(4), 40°(3), 65°(3), 115°(3), 140° (3), and 157°(3)] with respect to the beam axis (the number in the parentheses is the number of detectors at the respective angles). The fast digital data-acquisition system based on Pixie-16 modules from XIA [25] was used for collecting the in-beam data. About 4×10^9 two- and higher-fold γ-γ coincidence events were collected in list-mode format. The data-acquisition system has been described in detail in Ref. [23].

The time-stamped data was sorted into different symmetric and angle-dependent E_γ-E_γ matrices and symmetric E_γ-E_γ-E_γ cube using the Multi pARameter time-stamped based COincidence Search (MARCOS) program [23], developed at TIFR. The time window for the coincidence was chosen to be 100 ns. The E_γ-E_γ symmetric matrix and E_γ-E_γ-E_γ cube were analyzed using the INGASORT [26] and RADWARE [27,28] software packages. The relative efficiency and energy calibration of the detection system (INGA) were performed with the two radioactive sources ^{152}Eu and ^{133}Ba, placed at the target position of the INGA setup.

The multipolarities and the electromagnetic characters of the observed γ-ray transitions for assigning the spin parity of the levels were determined from the measurements of the of ratio for directional correlation from oriented state (DCO ratio) [29,30], angular distribution from oriented nuclei (ADO) ratio [31], and the linear polarization. The experimental details and data-analysis procedures have been described in detail in Refs. [13,32].

In the present investigation, the detectors at 140° and 90° with respect to the beam direction were used to evaluate the DCO ratios that were compared with the theoretical values [33] for multipolarity assignments of the γ-ray transitions. The theoretical DCO ratios for the observed γ transitions were calculated using the code ANGCOR [34]. Theoretically, for a stretched transition, the DCO ratio should be close to unity if the gating transition has the same multipolarity as that of the observed (analyzed) transition. The DCO ratios for a stretched dipole (quadrupole) transition gated by a pure quadrupole (dipole) transition are $\sim$0.5(2.0). For a mixed transition the DCO ratio depends on the detector angles, mixing ratio (δ), and the width of the substate population (σ/j) of the reaction.

To evaluate δ for a mixed transition from the measured DCO ratio, it is essential to estimate the value of σ/j for the present fusion-evaporation reaction. For this purpose, several pure electric dipole ($E1$) transitions of energy 1151.6 keV ($17/2^+ \rightarrow 15/2^-$) in ^{143}Eu [31] and 553.6 ($25/2^- \rightarrow 23/2^+$), 628.3 ($19/2^+ \rightarrow 17/2^-$), and 823.1 ($21/2^+ \rightarrow 19/2^-$) keV transitions in ^{141}Sm [21], populated in the same reaction, were selected. The DCO ratios were evaluated using a stretched $E2$ transition as the gating transition so that the gating and the observed (analyzed) transitions were both pure transitions of different multipolarities. The gate width was set sufficiently narrow to eliminate/minimize contaminations. The DCO ratios then compared with the values calculated using ANGCOR, with the spin alignment (σ/j) being varied as a parameter, to check for the best compliance. The DCO ratios calculated for different transitions, with varying values of σ/j are shown in Fig. 1. It can be seen from the figure (Fig. 1) that the experimental DCO ratios for the 1151.6-, 553.6-, 628.3-, and 823.1-keV γ transitions were reproduced with the width of the substate
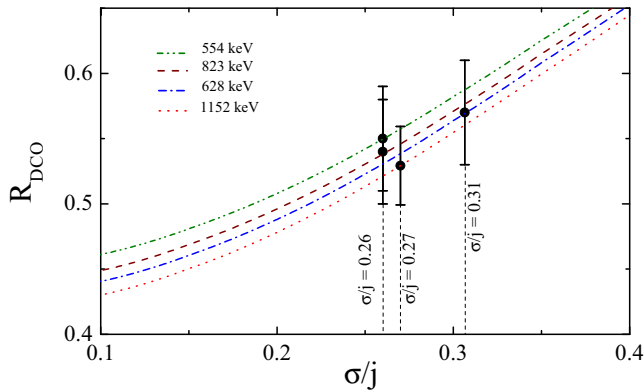
FIG. 1. Theoretical R_{DCO} values for different σ/j value of the reaction (represented by red, orange, olive, and black lines) for the present experimental setup, calculated using ANGCORprogram. Experimental R_{DCO} ratios for the 1151.6 ($17/2^+ \rightarrow 15/2^-$)-keV $E1$ transition in ^{143}Eu and 553.6 ($25/2^- \rightarrow 23/2^+$)-keV, 628.3 ($19/2^+ \rightarrow 17/2^-$)-keV, and 823.1 ($21/2^+ \rightarrow 19/2^-$)-keV $E1$ transitions in ^{141}Sm (represented by the solid circles), reproduced assuming $\sigma/j = 0.27$ and 0.26, 0.31, and 0.26, respectively.

population (σ/j) as 0.27, 0.26, 0.31, and 0.26, respectively. To calculate the mixing ratios (δ) for the transitions of the dipole structure in ^{141}Sm, we have thus adopted $\sigma/j = 0.27$, which is the weighted average of the aforesaid values.

As far as the ADO ratio (R_θ) values were concerned, they were 0.6 (1.6) for the stretched dipole (quadrupole) γ-ray transitions for the present experimental setup. The R_θ values of the mixed transitions deviate from those for the stretched condition. The values for the stretched transitions were determined from the transitions of known multipolarity in ^{142,143}Eu [31]. This procedure for assigning multipolarities is more effective than the DCO ratio measurements, particularly for the weak transitions and generally for the magic nuclei where the stretched transitions are rarely observed.

Definitive assignment of the spin parity of the excited levels can be done from the combined results of the DCO and the ADO analysis along with the linear polarization measurements for the observed γ-ray transitions. The clover detectors at 90° of the INGA setup were used for the linear polarization (P) measurement. The reference plane of the γ ray is defined by the plane which contains both the beam axis and the emission direction of the γ ray. Compton-scattered events in neighboring pairs of Ge crystals of the clover detectors, scattered horizontally and vertically to the reference plane, were distinguished in the sorting process for identification of their electromagnetic character. Two asymmetric E_γ-E_γ matrices were constructed for the purpose with the horizontally or vertically scattered γ rays (at 90° detectors) on one axis and the coincident γ-ray events from all other detectors on the second axis. The linear polarization asymmetry ratio [35–39] can be expressed as

$$A(E_\gamma) = \frac{a(E_\gamma)N_\perp - N_\parallel}{a(E_\gamma)N_\perp + N_\parallel}.$$

Here, $N_\parallel$ ($N_\perp$) denotes the number of the scattered events in the parallel (perpendicular) directions with respect to the reference plane, for a given γ-ray transition.

The asymmetry correction factor [$a(E_\gamma) = N_\parallel/N_\perp$], representing the geometrical asymmetry of the detection system (INGA setup), was determined by using the unpolarized radioactive ^{152}Eu and ^{133}Ba sources and found to be close to unity [0.98(0.02)] for the present experimental setup [13]. The linear polarization (P) of a γ-ray transition, polarization sensitivity (Q), and the polarization asymmetry (A) are related as $P = A/Q$. The Q values of the detection system have been taken from Ref. [13]. The positive, negative, and near-zero P values are expected for the γ-ray transitions of electric, magnetic, and mixed character, respectively.

III. EXPERIMENTAL RESULTS

The ^{141}Sm nucleus has been populated in the the heavy-ion fusion-evaporation reaction of ^{116}Cd (used as target) with ^{31}P as the projectile at an energy of 148 MeV. Several nuclei populated in this reaction, as depicted in the total projection spectrum of the E_γ-E_γ-E_γ cube [Fig. 2(a)]. This spectrum shows that, along with the strongly populated channels viz. ^{143}Eu and ^{142}Sm nuclei, the ^{141}Sm nucleus is populated with reasonable cross section ($\sim$10% of the total cross section). The double-gated spectrum created by the gatelist of energy 634.8, 1089.0, and 1418.0 keV shows almost all previously observed transitions of the band of interest along with the other transitions in ^{141}Sm [(Fig. 2(b)] [21,22]. This, in turn, reflects reasonable population of the desired band structure in the nucleus of interest.

The proposed partial level scheme of the dipole structure above the 3377-keV excitation energy in ^{141}Sm obtained from the present experiment, as shown in Fig. 3, was established using the coincidence relationship, relative intensity (I_γ), DCO ratio (R_{DCO}), R_θ, and P measurements. All the γ transitions of the dipole bands, previously observed by the Cardona *et al.* [22], were confirmed in the present investigation. The intensities of the γ transitions above the 3377-keV $25/2^-$ excited state in ^{141}Sm were determined from the symmetrized E_γ(90°)-E_γ(90°) matrix and normalized with the intensity of the 132.6-keV ($27/2^- \rightarrow 25/2^-$) γ transition. The γ-ray transition energies (E_γ), I_γ, R_{DCO}, R_θ, P, δ, and spin parities of the dipole structure of ^{141}Sm are given in Table I.

The R_{DCO} for the 132.6-keV transition is 1.31(0.11), indicating a mixed multipolarity, in contrast to the previous assignments. This value can be theoretically reproduced by considering the 132.6-keV transition both as a dipole with considerable amount of quadrupole admixture ($M1 + E2$ or $E1 + M2$) or a quadrupole with a small mixing of multipole order $L = 3$ (octupole), as shown in Fig. 4. Weisskopf estimate of the level lifetime of the state, depopulated by the 132.6-keV transition, is $\sim$ps for a mixed $M1 + E2$ or $E1 + M2$ transition and $\sim\mu$s in case of an $E2 + M3$ or $M2 + E3$ transition deexciting the state. The corresponding experimental level lifetime is $2.37^{+0.45}_{-0.39}$ ps (see Table II), which excludes the possibility of the 132.6-keV γ-ray transition being of $E2 + M3$ or $M2 + E3$ in nature and, consequently, a mixed $M1 + E2$ or $E1 + M2$ character, with a substantial quadrupole ($E2$ or $M2$) component, having a mixing ratio of 0.97(0.28), can be adopted for the transition.
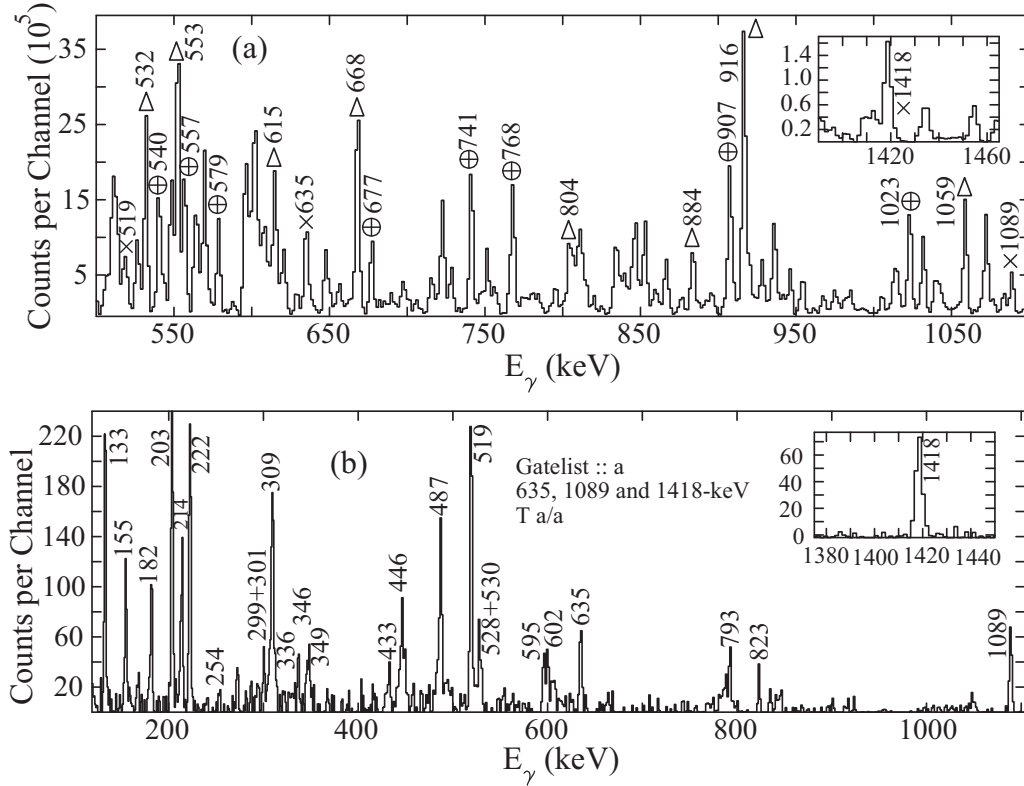
FIG. 2. In panel (a) total projection spectrum of the E_γ-E_γ-E_γ cube shows the γ rays of the nuclei populated in the present reaction. The peaks marked with the "Δ", "$\oplus$", and "$\times$" are the γ-ray transitions in ^{143}Eu, ^{142}Sm, and ^{141}Sm, respectively. The summed double-gated γ-ray spectrum of the 634.8-, 1089.0-, and 1418.0-keV γ transitions showing the γ rays in ^{141}Sm is displayed in panel (b).
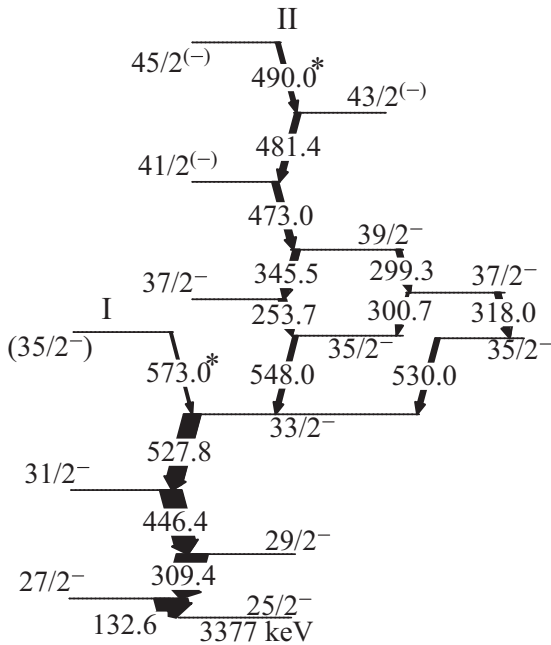

FIG. 3. The partial level scheme of ^{141}Sm obtained in the present work. The γ-ray energies are given in keV and the width of the arrows are proportional to the intensities of the transitions. The new γ transitions have been marked by asterisks.

To further resolve the nature of 132.6-keV γ transition, we have performed the angular distribution measurements for the same. The normalized experimental yield of the transition events [peak intensity] at various angles [$W(\theta)$] with respect to the beam axis was fitted with the Legendre polynomial function,

$$W(\theta) = A_0[1 + a_2 P_2(\cos\theta) + a_4 P_4(\cos\theta),$$

where a_2 and a_4 are the angular distribution coefficients [41,42]. Figure 5 shows the measured angular distribution along with the fitted values for the 132.6-keV γ transition. The fitted values of the a_2 and a_4 coefficients are $-0.19(0.03)$ and $-0.04(0.01)$, respectively, in compliance with a mixed $M1 + E2$ character.

To determine the mixing ratio from the measured a_2 and a_4 coefficients, we have calculated them theoretically considering a partial degree of alignment as described by Yamazaki [43] and by Mateosian and Sunyar [44]. In case of partial the alignment angular distribution coefficients are expressed as

$$a_k = \alpha_k A_k^{\max}.$$

Here, $A_k^{\max}$ is the angular distribution coefficient for complete alignment and it is defined as [43,44]

$$A_k^{\max}(J_i L_1 L_2 J_f)$$
$$= \frac{f_k(J_f L_1 L_1 J_i) + 2\delta f_k(J_f L_1 L_2 J_i) + \delta^2 f_k(J_f L_2 L_2 J_i)}{1 + \delta^2},$$

TABLE I. Energy (E_γ), relative intensity (I_γ), R_{DCO}, R_θ, linear polarization (P), mixing ratio (δ), and assignment of the γ transitions in ^{141}Sm.

E_γ[a]	I_γ[b]	J_i^π	J_f^π	R_{DCO}[c]	R_θ	P	δ	Assignment
132.6	100.0	$27/2^-$	$25/2^-$	1.31(0.11)	1.11(0.07)		0.97(0.28)	$M1/E2$
253.7	20.1(2.8)	$37/2^-$	$35/2^-$	0.72(0.09)	0.84(0.07)	−0.23(0.15)	0.13(0.08)	$M1$
299.3	11.5(1.8)	$39/2^-$	$37/2^-$		0.66(0.08)	−0.13(0.10)		$M1$
300.7	8.5(1.2)	$37/2^-$	$35/2^-$		0.75(0.09)	−0.15(0.11)		$M1$
309.4	94.1(5.1)	$29/2^-$	$27/2^-$	0.68(0.07)	0.63(0.05)	−0.13(0.09)	0.11(0.07)	$M1$
318.0	11.4(1.9)	$37/2^-$	$35/2^-$		0.78(0.09)	−0.21(0.15)		$M1$
345.5	18.4(2.1)	$39/2^-$	$37/2^-$	0.75(0.08)	0.81(0.06)	−0.12(0.10)	0.16(0.07)	$M1$
446.4	63.3(4.1)	$31/2^-$	$29/2^-$	0.77(0.10)	0.70(0.05)	−0.22(0.11)	0.18(0.08)	$M1$
473.0	18.3(3.5)	$41/2^{(-)}$	$39/2^-$		0.89(0.10)			$(M1)$
481.4	16.6(2.7)	$43/2^{(-)}$	$41/2^{(-)}$		0.92(0.09)			$(M1)$
490.0	11.2(2.1)	$45/2^{(-)}$	$43/2^{(-)}$		0.79(0.12)			$(M1)$
527.8	49.7(5.4)	$33/2^-$	$31/2^-$	0.81(0.10)	0.69(0.06)	−0.23(0.16)	0.22(0.09)	$M1$
530.0	12.6(1.9)	$35/2^-$	$33/2^-$		0.52(0.04)	−0.18(0.14)		$M1$
548.0	28.4(4.0)	$35/2^-$	$33/2^-$	0.79(0.08)	0.84(0.09)	−0.19(0.12)	0.20(0.07)	$M1$
573.0	6.8(1.8)	$(35/2^-)$	$33/2^-$					$(M1)$

[a]Uncertainty in γ-ray energy is $\pm(0.1$–$0.3)$ keV.
[b]Intensities of γ rays are corrected for the internal conversion and normalized to the 132.6-keV transition [40].
[c]DCO ratios are obtained from stretched $E2$ transition.

where, L_1 and L_2 are the angular momenta of the γ ray with $L_2 = L_1 + 1$ and δ is the mixing ratio of the γ ray. The values of the f coefficients are tabulated in Refs. [43,44] for different J_i values. The attenuation coefficient, α_k, depends on J and the distribution of the nuclear state over its m substates [43,44]. The mixing ratio (δ) has been extracted by comparing the ratio of the experimental angular distribution coefficients (a_2/a_4) with the theoretically calculated values (considering $\sigma/j = 0.27$), as shown in Fig. 6 and the value was found to be $1.17^{+0.41}_{-0.29}$. This value is in agreement with the value obtained from analysis of the R_{DCO} result. Thus, a spin-parity of $27/2^-$ was assigned to the state depopulated by the 132.6-keV transition.
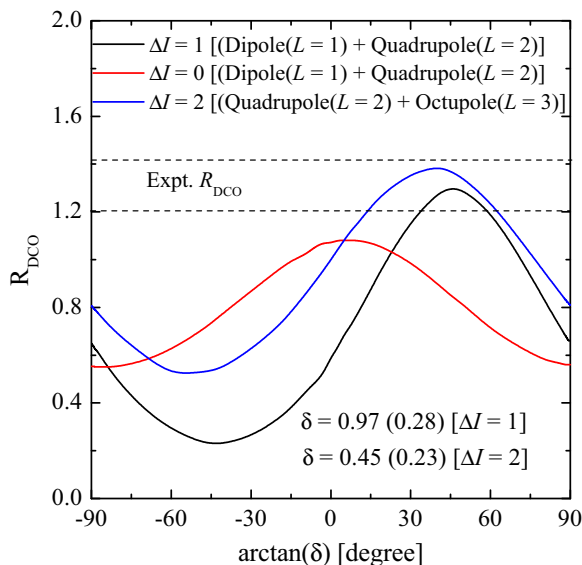

FIG. 4. The variation of R_{DCO} for with the mixing ratio (δ) of different multipoles (L) for the 132.6-keV transition in ^{141}Sm.

The nature of the 132.6-keV ($27/2^- \rightarrow 25/2^-$) transition could also be confirmed from the intensity balance. The 132.6-keV transition feeds the $25/2^-$ level, which decays through the 553.6 ($25/2^- \rightarrow 23/2^+$)- and 59.0 ($25/2^- \rightarrow 23/2^-$)-keV transitions (for a full level scheme, see [21,22]). In the present investigation the intensity of the 59.0-keV γ-ray transition could not be determined precisely as the clover detectors have insufficient γ-ray detection efficiency at low energy. For this reason the intensities of the transitions deexciting the $23/2^-$ level were measured and taken as the intensity of the 59.0-keV transition. Thus, the total intensity of the decaying out transitions for the $25/2^-$ level was compared with the intensity of the 132.6- and 203.4-keV transitions feeding it. The 203.4-keV transition was previously identified as a magnetic dipole in nature [21,22]. The measured total intensity of the transitions depopulating from the $25/2^-$ level is 36.1(4.2), whereas the intensities of the 203.4- and

TABLE II. Measured level lifetimes and corresponding $B(M1)$ values from the full clover detector for the dipole bands I and II in ^{141}Sm.

Band	I_i^π	E_γ (keV)	τ (ps)	$B(M1)\mu_N^2$
	$27/2^-$	132.6	$2.37^{+0.45}_{-0.39}$	$2.92^{+0.55}_{-0.48}$
I	$29/2^-$	309.4	$1.05^{+0.21}_{-0.18}$	$1.54^{+0.31}_{-0.26}$
	$31/2^-$	446.4	$0.72^{+0.15}_{-0.13}$	$0.75^{+0.16}_{-0.14}$
	$33/2^-$	527.8	$1.11^{+0.23}_{-0.15}$	$0.29^{+0.06}_{-0.04}$
	$35/2^-$	548.0	$0.40^{+0.08}_{-0.08}$	$0.72^{+0.14}_{-0.14}$
II	$37/2^-$	253.7	$1.88^{+0.40}_{-0.35}$	$1.45^{+0.31}_{-0.27}$
	$39/2^-$	345.5	1.15[a]	0.97[b]

[a]Effective lifetime is obtained assuming 100% side-feeding intensity. Hence, it is the upper limit of level lifetime (τ).
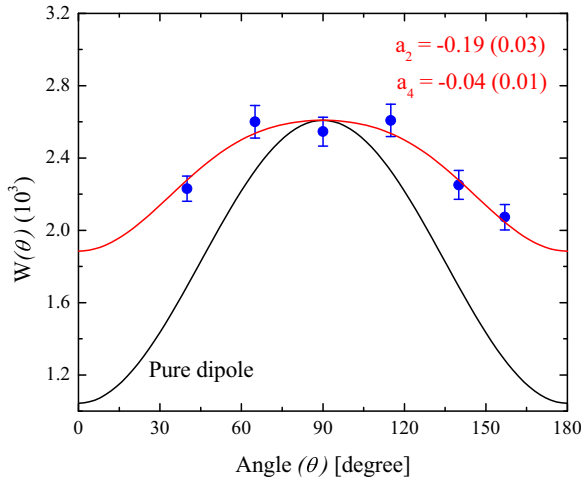[b]Lower limit of the $B(M1)$ value.

FIG. 5. Angular distribution of the 132.6-keV $(27/2^- \to 25/2^-)$ γ-ray transition in ^{141}Sm. The solid red line represents the fit to the experimental data points. The solid black line represents the angular distribution of a pure dipole transition.

132.6-keV transitions are 17.2(1.4) (including effect of the internal conversion [40]) and 9.8(1.1) (without considering the internal conversion), respectively. The intensities of the transitions have been normalized with the intensity of 634.8 keV $(15/2^- \to 11/2^-)$ transition as 100.0 [21,22]. The ratio of the maximum missing intensity to the observed intensity for the 132.6-keV transition is 0.93(0.18). This value is in agreement with the total internal conversion coefficient of $0.81^{+0.02}_{-0.01}$ for the $M1/E2$ ($\delta = 1.17^{+0.41}_{-0.29}$ as obtained from the present angular distribution measurement) mixed character of the 132.6-keV γ-ray transition [40]. The $E1/M2$ ($\delta = 1.17^{+0.41}_{-0.29}$) mixed nature of the 132.6-keV transition gives the total internal conversion coefficient of $3.42^{+0.98}_{-0.81}$, which is much higher than the measured value 0.93(0.18). Thus, the intensity balance measurements unambiguously established the $M1/E2$
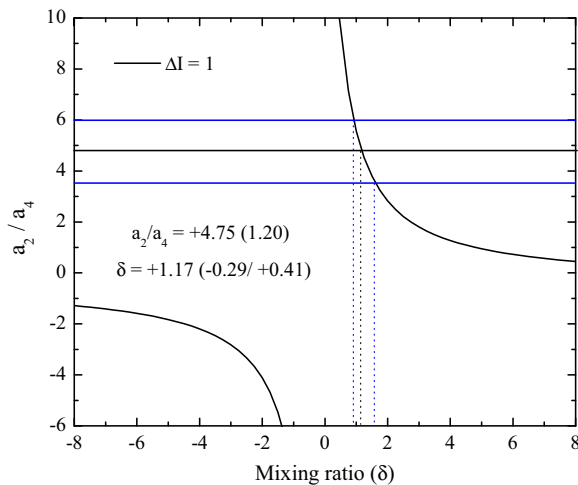

FIG. 6. Evolution of the ratio of the angular distribution coefficients (a_2/a_4) with mixing ratio (δ) for the 132.6-keV $(27/2^- \to 25/2^-)$ γ-ray transition in ^{141}Sm.

character of the 132.6-keV γ-ray transition at variance with the pure $M1$ assignment in the previous studies on the nucleus.

Measured values of $R_{\rm DCO}$, R_θ, P, and δ for the 309.4-, 446.4-, and 527.8-keV transitions indicate their magnetic dipole $M1$ nature with small $E2$ admixture. These measurements were in compliance with the earlier assignments done by the Lach *et al.* [21] and confirmed the spin parities of the levels up to the $33/2^-$ state. Above the $33/2^-$ excited state, Lach *et al.* [21] had observed the 548.1- and the 299.9-keV γ transitions only. However, Cardona *et al.* [22] proposed a complex structure above the $33/2^-$ level consisting of the 548-, 530-, 318, 300-, 300-, 254-, and 346-keV γ transitions up to the $39/2$ state without any parity assignment.

In the present experiment a weak transition of energy 573.0 keV has been observed in the sum of the double-gated spectra created by gatelist "a" of γ energies 132.6, 309.4, 446.4, and 527.8 keV (Fig. 7). The 573.0-keV transition remains unobserved in the double-gated spectrum produced by gatelist "a" and the 548.0-keV transition. Hence, the 573.0-keV transition has been placed above the 527.8-keV transition and parallel to the 548.0- and 530.0-keV γ transitions populating the $33/2^-$ state, as shown in Fig. 3. In addition, the double-gated spectrum created by gatelist "a" and the 573.0-keV transition shows all γ-ray transitions of gatelist "a", thus corroborating the placement of the 573.0-keV transition above the 527.8-keV transition. The intensity of the 573.0-keV transition is too weak for performing the $R_{\rm DCO}$, R_θ, and P measurements. We have tentatively assigned the 573.0-keV transition as a dipole transition, and the state depopulating through the 573.0-keV transition has been tentatively assigned a spin parity of $(35/2^-)$. The cascade consisting of the 132.6-, 309.4-, 446.4-, 527.8-, and 573.0-keV γ-ray transitions has been designated as dipole band I, as shown in Fig. 3. It has been observed that the 253.7- and the 345.5-keV transitions remain absent in the sum spectrum of the double gates on the 299.3- or 300.7-keV transition and one of the 132.6-, 309.4-, 446.4-, and 527.8-keV transitions, thus upholding the level structure proposed by Cardona *et al.* [22]. The values of $R_{\rm DCO}$, R_θ, P, and δ for the 548.0-, 253.7-, and 345.5-keV γ transitions established their $M1/E2$ mixed character and the corresponding states were assigned spin parity $35/2^-$, $37/2^-$, and $39/2^-$, respectively. The measured R_θ and P values for the 530.0- and 318.0-keV transitions indicate their magnetic dipole ($M1$) character and the states decaying through these transitions have been designated as $35/2^-$ and $37/2^-$, respectively. For the 473.0- and 481.4-keV transitions we could only measure the R_θ values that are commensurate with their $\Delta I = 1$, dipole character. Hence, the corresponding states were tentatively assigned as $41/2^{(-)}$ and $43/2^{(-)}$, respectively.

Above the $43/2^{(-)}$ excited level a new γ-ray transition of energy 490.0 keV was observed (Fig. 7). For the 490.0-keV transition we could not determine the values of $R_{\rm DCO}$ and P. However, the measured R_θ value of the transition indicated a dipole character and the spin-parity of the corresponding state was assigned as $45/2^{(-)}$. The dipole structure, starting from the $35/2^-$ to the $45/2^{(-)}$ state, constituted with the dipole transitions of energies 253.7, 345.5, 473.0, 481.4, and 490.0 keV has been labeled as dipole band II (Fig. 3).
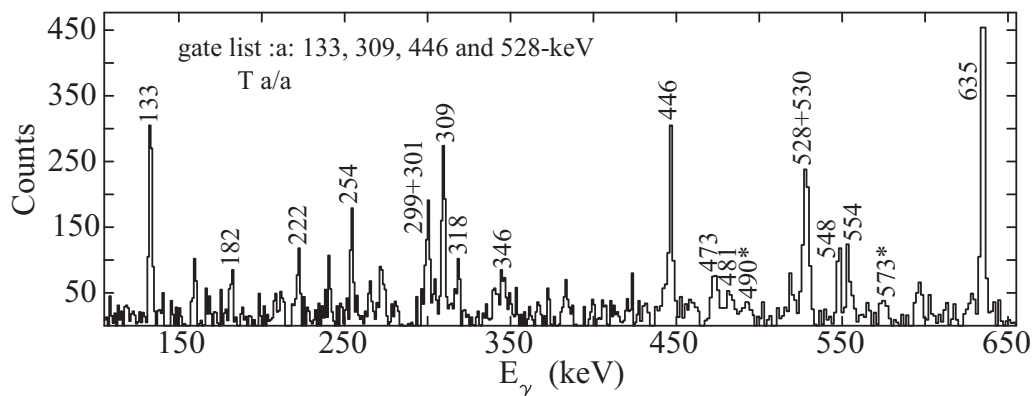
FIG. 7. Summed double-gated γ-ray spectrum of the 132.6-, 309.4-, 446.4-, and 527.8-keV γ transitions shows the γ rays in ^{141}Sm. The peaks marked with the asterisks are the newly observed member of dipole bandlike structures in ^{141}Sm.

Doppler-broadened line shapes were observed for the transitions of the dipole structures in ^{141}Sm above the $I^{\pi} = 25/2^{-}$ up to the $39/2^{-}$ state. The level lifetimes of the states of the dipole structure were extracted using the LINESHAPE code of Wells and Johnson [45,46]. The energy loss and the trajectories of the residual nuclei (^{141}Sm) in time steps of 1.5 fs while traversing inside the target and/or backing medium was simulated using Monte Carlo techniques with electronic stopping powers calculated from the shell-corrected tabulations of Northcliffe and Schilling [47] and nuclear stopping powers from the theory of Linhard, Schraff, and Schiott [48]. The velocity profiles of the residual nuclei (^{141}Sm) for the clover detectors at different angles were then generated by assuming that the response of a composite clover detector was identical to a single-crystal high-purity germanium (HPGe) detector with the dimension same as the dimension of the former placed at the same distance. The validity of this assumption was checked by analyzing the Doppler shapes obtained from a single crystal of a particular clover detector in the array [32] and comparing the lifetime results with that obtained from using the clover. The LINESHAPE program uses the velocity profiles to calculate the Doppler shape for a γ transition. The lifetime of the corresponding state is then extracted from fitting the calculated shape to the experimental one. The process of line-shape fitting was described in detail in Refs. [13,32]. For the present analysis, E_{γ}-E_{γ} asymmetric matrices were used to construct the background-subtracted gated spectra for different angles. The gates were set on the transitions below the band of interest. The gate on the transitions below the transitions of interest necessitates to consider the side-feeding contribution. The side feeding has been modeled with a cascade of five transitions having the same moment of inertia as that of the band under consideration [46]. Initially, starting from the topmost transition, the members of the band have been sequentially fitted. After having fitted all the transitions of the band, sequentially, a global least-squares minimization has been carried out for all the transitions of the cascade simultaneously, wherein only the transition quadrupole moments and the side-feeding quadrupole moments for each state have been kept as free parameters. To find out the effect of side feeding on the evaluated lifetimes, we vary the side-feeding intensities between two extreme values (taking the corresponding uncertainties in intensities into account). The effect of variation in the side-feeding intensity resulted in a change in the level lifetime by less than 15% [13]. The spectra at $65°$, $90°$, and $140°$ were fitted simultaneously to extract the level lifetimes.

We have obtained the level lifetimes of seven levels ($39/2^{-}$ to $27/2^{-}$) of the dipole bands I (four levels depopulating via the 132.6-, 309.4-, 446.4-, and 527.8-keV γ transitions) and II (three levels decaying through the 548.0-, 253.7-, and 345.5-keV transitions) in ^{141}Sm. Typical fits to the observed Doppler shapes for the transitions of the dipole bands I and II in ^{141}Sm are shown in Fig. 8. The 345.5-keV γ transition ($39/2^{-} \rightarrow 37/2^{-}$) in dipole band II is the topmost transition of the dipole structure for which a clear line shape has been observed in the experimental spectra, wherefrom an effective lifetime of 1.15 ps has been obtained for the state. This was used to calculate the lifetime of the next lower state $37/2^{-}$. The lifetime analysis of the next lower level $35/2^{-}$, decaying through 548.0-keV transition, needs to be elaborated. The level is fed by two independent transitions, 253.7 and 300.7 keV, both de-exciting $37/2^{-}$ levels and both exhibiting Doppler shape. Thus, both of these transitions need to be incorporated in the feeding history of the $35/2^{-}$ state. The level lifetime of the $37/2^{-}$ deexcited by the 253.7-keV transition was determined as per the procedure discussed above, whereas the lifetime determination of the other $37/2^{-}$ state, depopulated by the 300.7-keV transition, was obscured by the presence of the overlapping 299.3-keV transition. The 299.3- and 300.7-keV transitions were then fitted together, with the lifetime of the $39/2^{-}$, deexcited by the 299.3-keV transition, kept fixed at the value obtained from analyzing the 345.5-keV transition and the lifetime of the $37/2^{-}$ state decaying through the 300.7-keV transition was obtained. Finally, the intensity-weighted average of the level lifetime of the two $37/2^{-}$ states, decaying through 253.7- and 300.7-keV transitions, was used as the feeding time for the $35/2^{-}$ level and its lifetime was obtained from analysis of the 548.0-keV transition.

The level lifetimes and the corresponding $B(M1)$ values for the levels of the dipole band are given in Table II. We could not observe the Doppler shapes of the 530.0-, 318.0-, 473.0-, 481.4-, and 490.0-keV transitions (maybe owing to their insufficient statistics). Uncertainties in the calculated
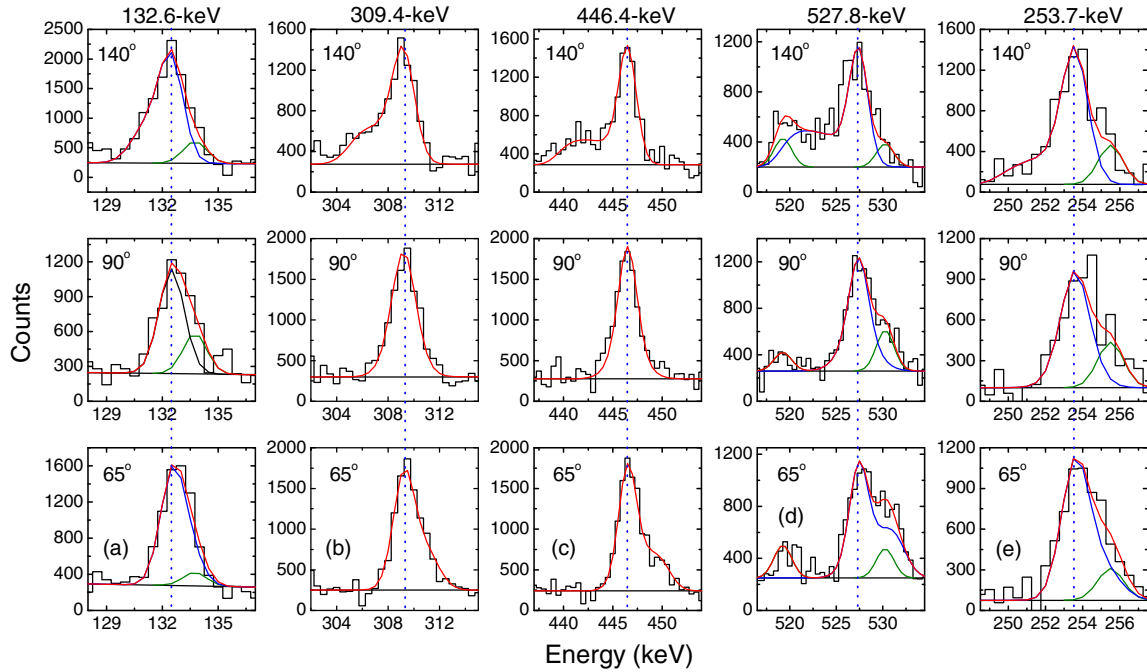
FIG. 8. The experimental observed spectra along with the fitted line shapes for the dipole transitions (a) 132.6, (b) 309.4, (c) 446.4, (d) 527.8, and (e) 253.7 keV of the dipole bands I and II in ^{141}Sm. The top, middle, and bottom rows correspond to the shapes in the 140°, 90°, and 65° detectors, respectively. The obtained line shape of the γ transition, contaminant peaks, and total line shapes are represented by the blue, olive, and red curves, respectively. The vertical dotted lines represent the stopped peak position for each transition whose shape is observed.

level lifetimes have been derived from the character of the χ^2 fit in the vicinity of the minimum. The systematic errors owing to the uncertainty in the stopping power of the target/backing medium, which can be as large as 15%, have not been included in the quoted errors of the level lifetimes.

IV. DISCUSSION

A sequence of dipole transitions with the regular energy spacing was observed up to the state having spin parity $I^\pi = (35/2^-)$ starting from the $I^\pi = 25/2^-$ of dipole band I in ^{141}Sm. Similar dipole bands had been observed in the neighboring nuclei ^{139,142}Sm, ^{141,143}Eu, and ^{142}Gd. These dipole bands have been identified as MR bands on the basis of the characteristic decrease of the $B(M1)$ values with spin along the bands [13–15,20,32]. The evaluated $B(M1)$ values for the states in the dipole band I of ^{141}Sm are comparable to the dipole bands in ^{139,142}Sm, ^{141,143}Eu, and ^{142}Gd [13–15,20,32] and the $B(M1)$ values have also been found to decrease with increase in the excitation energy along the dipole band I (Table II). This characteristic decrease of the $B(M1)$ values [Fig. 9(a)] may be attributed to the fact that the states in the dipole band I have been originated from the shears mechanism.

For better understanding of the intrinsic structure of the dipole bands I and II in ^{141}Sm we have performed a semiclassical-model calculation within the framework of SPAC model [13–15]. In this model, the shears angular momentum $(\vec{j}_{\rm sh})$, produced by the holes and the particle angular momenta, is coupled with the angular momentum vector $\vec{R}$ of the collective rotation to generate the total spin of

the observed state (I). The total energy of an excited state $E(I)$ can be expressed by the sum of the collective and quasiparticle (shears) energy contribution as

$$E(I) = E(\text{core}) + E(\text{shears}) + \text{constant}.$$

Here,

$$E(\text{core}) = \frac{R^2(I, \theta_1, \theta_2)}{2J(I)}$$

is the energy owing to rotation of the core and

$$E(\text{shears}) = v_2 P_2[\cos(\theta_1 - \theta_2)]$$

is the quasiparticle energy owing to the interaction between the shear angular momenta $\vec{j}_1$ and $\vec{j}_2$. Here, θ_1 and θ_2 are the angles of $\vec{j}_1$ and $\vec{j}_2$ with respect to the rotational axis, respectively. Generally, for each value of I, θ_1, and θ_2 can be found from the energy minimization condition,

$$\frac{\partial^2 E(I, \theta_1, \theta_2)}{\partial \theta_1 \partial \theta_2} = 0.$$

For a normal initial alignment [15], the direction of $\vec{j}_2$ is set along the rotational axis and the two-dimensional energy minimization condition can be replaced by the one-dimensional condition,

$$\frac{\partial E(I, \theta_1)}{\partial \theta_1} = 0,$$

which is then used to obtain θ_1 for the excited state with angular momentum I.
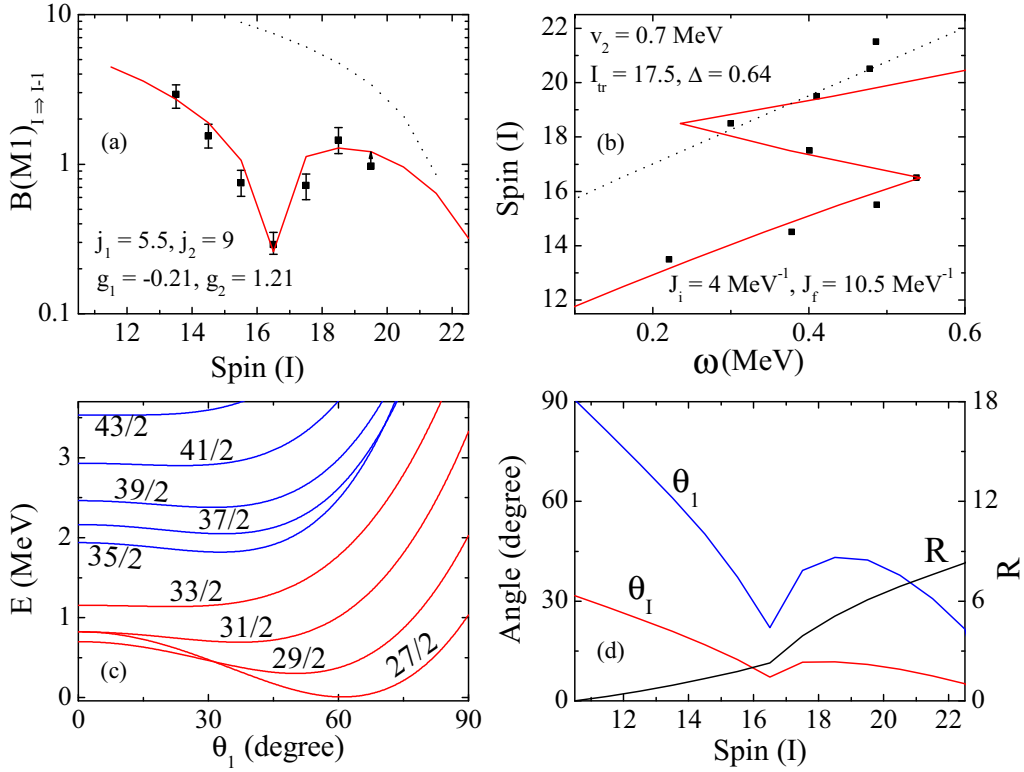
FIG. 9. Comparison of the experimental results (represented by solid squares) for the dipole bands I and II in ^{141}Sm in the framework of the SPAC-model (solid lines) calculations. In panel (a) $B(M1)$ transition strengths against spin (I); (b) angular momentum (I) vs $\hbar\omega$; (c) energy of the excited states as a function of θ_1; and (d) evolution of the angle θ_1 (solid blue line), θ_I (solid red line), and collective core rotational angular momentum (R) (solid black line) against spin for the dipole bands are shown. Here, θ_I is the angle between the total angular momentum vector (I) and the collective core rotational angular momentum (R). The parameters used for the calculations are given in the figures. The dotted lines represent the SPAC-model calculations for dipole band II assuming $j_1 = 10.5\hbar$, $j_2 = 9\hbar$, and $J = 4.1 \ \hbar^2/\text{MeV}$ (see text for details).

The collective core rotational angular momentum ($\vec{R}$) and core moment of inertia $J(I)$ are assumed to be I dependent and have been described in the band-crossing region by Boltzmann or Hill function [49].

The odd mass $N = 79 \ ^{139}$Nd [50,51], ^{141}Sm [21,22], and ^{143}Gd [52] nuclei in mass $A \sim 140$ region show the dipole cascades above the $25/2^-$ state at excitation energies 3.8, 3.4, and 3.1 MeV, respectively. In addition, there exist the dipole bands above the same spin state in odd mass $N = 77 \ ^{139}$Sm [20] and $N = 78 \ ^{141}$Eu [15] at the excitation energies 3.3 and 2.8 MeV, respectively. Among these dipole bands the dipole bands in ^{139}Sm and ^{141}Eu have been identified as MR band with configurations $\pi h_{11/2}^2 \otimes \nu h_{11/2}^{-1}$ and $\pi h_{11/2}^1 \otimes \nu h_{11/2}^{-2}$, respectively [15,20]. Thus, for odd mass nuclei in the $A \sim 140$ region the dipole bands with bandhead energy ≈ 3.0 MeV may have three-quasiparticle (three quasiparticles in $h_{11/2}$ orbitals) configuration. Hence, the configuration of the observed dipole band I with bandhead energy 3377 keV in ^{141}Sm has been assumed as $\pi h_{11/2}^2 \otimes \nu h_{11/2}^{-1}$. With this configuration the bandhead spin can be reproduced with a small core contribution ($1\hbar$).

The SPAC-model calculations have been carried out with the configuration $\pi h_{11/2}^2 \otimes \nu h_{11/2}^{-1}$ for the dipole band I in ^{141}Sm. To understand the shape of the ^{141}Sm nucleus associated with this configuration, total Routhian surface (TRS)

calculations [53,54] have been performed. The contour plots of the TRS calculations of the above-mentioned configuration for the dipole band I are presented in Fig. 10(a). It can be seen from Fig. 10(a) that the dipole band I in ^{141}Sm has a minimum at prolate deformation with $\beta_2 \approx 0.15$ that has been considered for the SPAC-model calculations with normal initial alignment [13–15]. Under this assumption, angular momenta generated by the particles and holes are rotation and deformation aligned, respectively. The energy has been minimized for the dipole band assuming the above-mentioned configurations and normal initial alignment. The calculations have been performed assuming an unstretched condition of the angular momenta with $j_1 = 5.5\hbar$, $j_2 = 9\hbar$, $g_1 = -0.21$, and $g_2 = +1.21$ for the dipole band [13,14]. Under these assumptions, the energy levels, spins(I), and the $B(M1)$ values for the dipole band I were well reproduced. For initial normal alignment the spin dependence of θ_1, θ_I, and R are shown in Fig. 9(d). The experimental dipole transition strength $B(M1)$ against the spin of the states and the angular momenta are plotted against the rotational frequency ($\hbar\omega$) along with the calculated values, as shown in Figs. 9(a) and 9(b).

It can be seen from Fig. 9(a) that the experimental $B(M1)$ value decreases from $2.92^{+0.55}_{-0.48}\mu_N^2$ to $0.29^{+0.06}_{-0.04}\mu_N^2$ for the $I^\pi = 27/2^-$ to $I^\pi = 33/2^-$ excited levels, respectively, and the SPAC calculations well reproduce the experimental
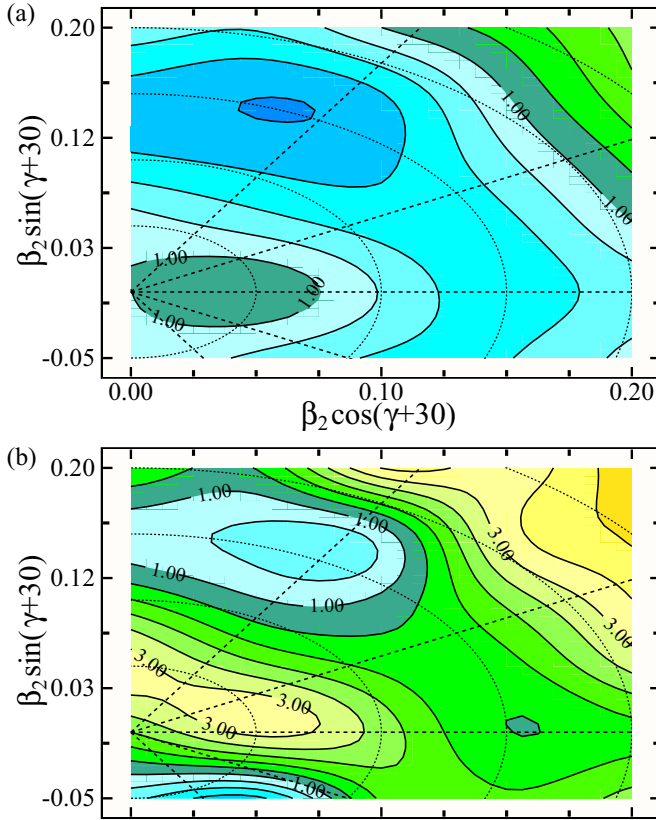
FIG. 10. Contour plots of the TRS calculations for the (a) $\pi h_{11/2}^2 \otimes \nu h_{11/2}^{-1}$ and (b) $\pi h_{11/2}^2 \otimes \nu h_{11/2}^{-3}$ configurations of the dipole bands I and II, respectively, in ^{141}Sm. The rotational frequency ($\hbar\omega$) for the calculations are (a) 0.170 and (b) 0.210 MeV. The energy difference between two contours is 0.400 MeV.

results with the configuration $\pi h_{11/2}^2 \otimes \nu h_{11/2}^{-1}$. For the $I^\pi = 35/2^-$ state the calculation predicts very small $B(M1)$ value ($\approx 0.0 \mu_N^2$), which may be attributable to the fact that at this point the shears angular momentum vectors are almost parallel. As a result, the transverse component of the magnetic dipole moment ($\mu_\perp$) rotating around the total angular momentum vector vanishes. So, no higher spin can be generated above the $I = 35/2$ from the configuration ($\pi h_{11/2}^2 \otimes \nu h_{11/2}^{-1}$) assigned for the dipole band I. The 573.0-keV transition above the $33/2^-$ state represents the termination of the dipole band I at a spin 35/2 state owing to the complete alignment of the two angular momentum blades.

The experimental $B(M1)$ values as well as rotational frequencies (ω) of the dipole band I have been reproduced well assuming that the particle pair is initially not fully stretched. The successful interpretation of the experimental results in the framework of the SPAC model indicates that the dipole band I in ^{143}Sm has been generated by the shears mechanism.

To reproduce the energy of the states above the $I^\pi = 33/2^-$ state of dipole band II a new configuration $\pi h_{11/2}^2 \otimes \nu h_{11/2}^{-3}$ has been proposed for the SPAC-model calculations. The TRS calculations show that the ^{141}Sm nucleus has a prolate shape ($\beta_2 \sim 0.16$) for this configuration [Fig. 10(b)]. The SPAC-model calculations for the dipole band II have been performed

for different unstretched conditions of the angular momenta values of j_1 and j_2 for the configuration $\pi h_{11/2}^2 \otimes \nu h_{11/2}^{-3}$, keeping the core contribution the same as the dipole band I ($J \sim 4.0 \hbar^2$/MeV). The calculation cannot reproduce the experimental $B(M1)$ and spin values simultaneously, as shown by the dotted lines in Figs. 9(a) and 9(b), respectively. These calculations were performed using $j_1 = 10.5\hbar$, $j_2 = 9\hbar$, and $J = 4.1 \, \hbar^2$/MeV. It is also apparent from Fig. 9(a), that the $B(M1)$ values above the $I_\pi = 33/2^-$ state, i.e., for the dipole band II cannot be cloned with the above assumptions in the framework of the SPAC model. This clearly indicates that the dipole band II may not be originated solely from multiquasiparticle excitation with the insignificant or zero core contribution. Therefore, the core contribution for the dipole band II has been included in the SPAC-model calculations by varying the core moment of inertia (J), as described in Ref. [49]. Using this technique, the energy levels and $B(M1)$ values above the $I^\pi = 33/2^-$ state are well reproduced from one-dimensional minimization condition as shown in Figs. 9(c) and 9(a), respectively. These calculations for the dipole band II show that a considerable amount of angular momentum is generated from the rotation of core [Fig. 9(d)]. This reflects in the slow decrease of the $B(M1)$ values of this band in comparison to the band I. However, the SPAC-model calculations for the dipole band II cannot reproduce the rapid increase of experimental spin (I) against the rotational frequency ($\hbar\omega$) above the $39/2^-$ state [Fig. 9(d)]. Such an increase of spin (I), in turn, reflects the rapid increase of the collective rotational angular momentum ($\vec{R}$) as shown in Fig. 9(b). The $B(M1)$ rates of the transitions for these states might encode the structural data and/or changes occurring in this spin region. However, the $B(M1)$ transition probabilities could be measured only for the three lower states in the band II with the value at $39/2^-$ being only an effective one. Hence, the reason behind the observed rapid increase of collectivity above the $39/2^-$ state could not be understood from the present experimental results.

The experimentally observed spins (I) of the selected MR bands in Sm, Eu, and Gd [13,14,20,32] isotopes have been shown in Fig. 11. The spins (I) grow smoothly with the increase of rotational frequency except in the case of ^{139}Sm and ^{141}Sm nuclei. In ^{139}Sm nucleus, much spin is generated with very little or no increase in the rotational frequency at the end of the band. This implies a gradual increase in the collectivity in the along the band. The TAC calculations for the MR band in ^{139}Sm show that the experimental results are better reproduced with the proposition that the collective angular momentum is increasing with rotational frequency and rotation around the intermediate axis (triaxial deformed shape) may exist at the high-spin region of the band [20]. In fact, the experimental $B(M1)$ values can be well described for $\gamma = 0°$ at low spins but at higher spins the agreement is better for $\gamma = -25°$, indicating that the γ deformation is changing with angular momentum in ^{139}Sm. A substantial amount of triaxiality has been reported in ^{128}Ba also [18]. Similar situation may arise in the case of ^{141}Sm. In this case the spins of the states against rotational frequency show a backbending followed by sudden increase of collectivity at the end of the band. However, further investigation is needed to
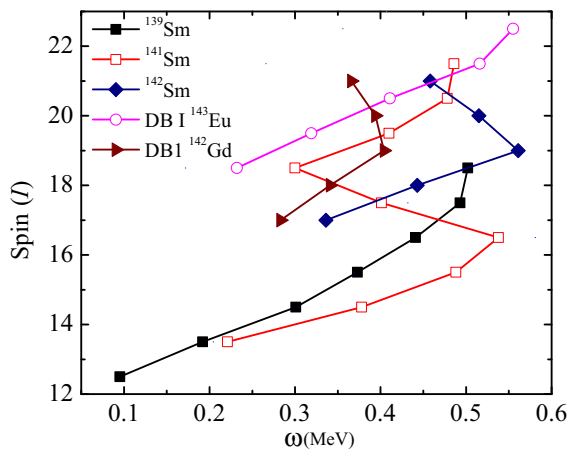
FIG. 11. The experimental angular momentum as a function of the rotational frequency for the MR bands of Sm, Eu, and Gd [13,14,20,32] nuclei in the $A \sim 140$ mass region.

explore the structure of the states above the $39/2^-$ state (band II) in ^{141}Sm, for conclusive interpretation.

V. SUMMARY

In summary, high-spin dipole structures in ^{141}Sm have been investigated using the reaction ^{116}Cd (^{31}P , $p5n$). The dipole nature of these bands has been confirmed from the DCO ratio, anisotropy, and linear polarization measurements of the intraband γ-ray transitions. The level lifetimes of the dipole bands I and II have been measured using the DSAM technique. The deduced experimental $B(M1)$ values have been compared with the SPAC-model calculations using the configuration $\pi h_{11/2}^2 \otimes \nu h_{11/2}^{-1}$ for the dipole band I that well reproduces the experimental results. From the characteristic decrease of the $B(M1)$ values along band I in ^{141}Sm and the reproduction of this trend in the model calculations, this band has been interpreted to be originating from the shears mechanism.

Level lifetimes of the higher-lying states in band II could not be extracted from the present data. However, a sharp increase in the spin with an insignificant increase in the rotational frequency in the higher spin domain of this band possibly indicate a development of collectivity similar to that observed in the neighboring ^{139}Sm nucleus. Lifetime measurements of these states would aid in confirming this proposition and can be pursued in a future investigation.

[1] R. M. Clark and A. O. Macchiavelli, Annu. Rev. Nucl. Part. Sci. **50**, 1 (2000).

[2] A. Bohr and B. R. Mottelson, Phys. Rev. **90**, 717 (1953).

[3] A. Bohr and B. R. Mottelson, *Nuclear Structure* (Benjamin, New York, 1975), Vol. II.

[4] S. Frauendorf, Rev. Mod. Phys. **73**, 463 (2001).

[5] R. Schwengner *et al.*, Phys. Rev. C **66**, 024310 (2002).

[6] D. G. Jenkins *et al.*, Phys. Lett. B **428**, 23 (1998).

[7] R. M. Lieder *et al.*, Eur. Phys. J. A **13**, 297 (2002).

[8] A. K. Singh *et al.*, Nucl. Phys. A **707**, 3 (2002).

[9] H. Hübel, Prog. Part. Nucl. Phys. **54**, 1 (2005).

[10] Amita, A. K. Jain, and B. Singh, At. Data Nucl. Data Tables **74**, 283 (2000).

[11] S. Frauendorf, Nucl. Phys. A **557**, 259c (1993).

[12] S. Frauendorf, Nucl. Phys. A **677**, 115 (2000).

[13] S. Rajbanshi, A. Bisoi, S. Nag, S. Saha, J. Sethi, T. Trivedi, T. Bhattacharjee, S. Bhattacharyya, S. Chattopadhyay, G. Gangopadhyay, G. Mukherjee, R. Palit, R. Raut, M. Saha Sarkar, A. K. Singh, and A. Goswami, Phys. Rev. C **89**, 014315 (2014).

[14] A. A. Pasternak *et al.*, Eur. Phys. J. A **23**, 191 (2005).

[15] E. O. Podsvirova *et al.*, Eur. Phys. J. A **21**, 1 (2004).

[16] H. Schnare, R. Schwengner, S. Frauendorf, F. Donau, L. Kaubler, H. Prade, A. Jungclaus, K. P. Lieb, C. Lingk, S. Skoda, J. Eberth, G. de Angelis, A. Gadea, E. Farnea, D. R. Napoli, C. A. Ur, and G. LoBianco, Phys. Rev. Lett. **82**, 4408 (1999).

[17] I. Schneider, R. S. Chakrawarthy, I. Wiedenhover, A. Schmidt, H. Meise, P. Petkov, A. Dewald, P. von Brentano, O. Stuch, K. Jessen, D. Weisshaar, C. Schumacher, O. Vogel, G. Sletten, B. Herskind, M. Bergstrom, and J. Wrzesinski, Phys. Rev. C **60**, 014312 (1999).

[18] O. Vogel, A. Dewald, P. von Brentano, J. Gableske, R. Krucken, N. Nicolay, A. Gelberg, P. Petkov, A. Gizon, J. Gizon, D. Bazzacco, C. Rossi Alvarez, S. Lunardi, P. Pavan, D. R. Napoli, S. Frauendorf, and F. Donau, Phys. Rev. C **56**, 1338 (1997).

[19] P. Petkov *et al.*, Nucl. Phys. A **640**, 293 (1998).

[20] A. A. Pasternak, E. O. Lieder1, R. M. Lieder, S. Chmel, W. Gast, Ts. Venkova, G. de Angelis, D. R. Napoli, A. Gadea, D. Bazzacco, R. Menegazzo, S. Lunardi, and G. Duchêne, Eur. Phys. J. A **37**, 279 (2008).

[21] M. Lach, P. Kleinheinz, J. Blomqvist, A. Ercan, H. J. Haihn, D. Wahner, R. Julin, M. Zupancic, F. Cigoroglu, and G. de Angelis, Z. Phys. A **345**, 427 (1993).

[22] M. A. Cardona, G. de Angelis, D. Bazzacco, M. De Poli, and S. Lunardi, Z. Phys. A **340**, 345 (1991).

[23] R. Palit, S. Saha, J. Sethi, T. Trivedi, S. Sharma, B. S. Naidu, S. Jadhav, R. Donthi, P. B. Chavan, H. Tan, and W. Hennig, Nucl. Instrum. Methods A **680**, 90 (2012).

[24] R. Palit *et al.*, J. Phys. Conf. Proc **420**, 012159 (2013).

[25] H. Tan *et al.*, in *Nuclear Science Symposium Conference Record 2008* (IEEE, Washington, DC, 2008), p. 3196.

[26] R. K. Bhowmik, Ingasort Manual (private communication).

[27] D. C. Radford, Nucl. Instrum. Methods Phys. Res., Sect. A **361**, 297 (1995).

[28] D. C. Radford, Nucl. Instrum. Methods Phys. Res., Sect. A **361**, 306 (1995).

[29] A. Krämer-Flecken, T. Morek, R. M. Lieder, W. Gast, G. Hebbinghaus, H. M. Jäger, and W. Urban, Nucl. Instrum. Methods Phys. Res., Sect. A **275**, 333 (1989).

[30] M. K. Kabadiyski, K. P. Lieb, and D. Rudolph, Nucl. Phys. A **563**, 301 (1993).

[31] M. Piiparinen, A. Atac, J. Blomqvist, G. B. Hagemann, B. Herskind, R. Julin, S. Juutinen, A. Lampinen, J. Nyberg, G. Sletten, P. Tikkanen, S. Tormanen, A. Virtanen, and R. Wyss, Nucl. Phys. A **605**, 191 (1996).

[32] S. Rajbanshi, A. Bisoi, S. Nag, S. Saha, J. Sethi, T. Bhattacharjee, S. Bhattacharyya, S. Chattopadhyay, G. Gangopadhyay, G. Mukherjee, R. Palit, R. Raut, M. Saha Sarkar, A. K. Singh, T. Trivedi, and A. Goswami, Phys. Rev. C **90**, 024318 (2014).

[33] K. S. Krane, R. M. Steepen, and R. M. Wheeler, Nucl. Data Tables **11**, 351 (1973).

[34] E. S. Macias, W. D. Ruhter, D. C. Camp, and R. G. Lanier, Comput. Phys. Commun. **11**, 75 (1976).

[35] K. Starosta, T. Morek, Ch. Droste, S. G. Rohozinski, J. Srebrny, A. Wierzchucka, M. Bergstrom, B. Herskind, E. Melby, T. Czosnyka, and P. J. Napiorkowski, Nucl. Instrum. Methods, Phys. Res. A **423**, 16 (1999).

[36] Ch. Droste, S. G. Rohoziiiski, K. Starosta, T. Morek. J. Srebrny, and P. Magierskib, Nucl. Instrum. Methods Phys. Res. A **378**, 518 (1996).

[37] J. K. Deng, W. C. Ma, J. H. Hamilton, A. V. Ramayya, J. Rikovska, N. J. Stone, W. L. Croft, R. B. Piercey, J. C. Morgan, and P. F. Mantica, Jr., Nucl. Instrum. Methods Phys. Res. A **317**, 242 (1992).

[38] P. M. Jones, L. Wei, F. A. Beck, P. A. Butler, T. Byrski, G. Duchne, G. de France, F. Hannachi, G. D. Jones, and B. Kharraja, Nucl. Instrum. Methods Phys. Res. A **362**, 556 (1995).

[39] R. Palit, H. C. Jain, P. K. Joshi, S. Nagaraj, B. V. T. Rao, S. N. Chintalapudi, and S. S. Ghugre, Pramana **54**, 347 (2000).

[40] T. Kibedi *et al.*, Nucl. Instrum. Methods Phys. Res., Sect. A **589**, 202 (2008).

[41] L. C. Biedenharn and M. E. Rose, Rev. Mod. Phys. **25**, 729 (1953).

[42] K. S. Krane and R. M. Steffen, Phys. Rev. C **2**, 724 (1970).

[43] T. Yamazaki, Nucl. Data, Sect. A **3**, 1 (1967).

[44] E. D. Mateosian and A. W. Sunyar, At. Data Nucl. Data Tables **13**, 391 (1974).

[45] J. C. Wells and N. R. Johnson, LINESHAPE: A Computer Program for Doppler Broadened Lineshape Analysis, Report No. ORNL-6689, 44, 1991.

[46] N. R. Johnson, J. C. Wells, Y. Akovali, C. Baktash, R. Bengtsson, M. J. Brinkman, D. M. Cullen, C. J. Gross, H.-Q. Jin, I.-Y. Lee, A. O. Macchiavelli, F. K. McGowan, W. T. Milner, and C.-H. Yu, Phys. Rev. C **55**, 652 (1997).

[47] L. C. Northcliffe and R. F. Schilling, Nucl. Data Tables A **7**, 233 (1970).

[48] Linhard, Schraff, and Schiott, Mat.-Fys. Medd.-K. Dan. Vidensk. Selsk. **33**, 14 (1963).

[49] A. A. Pasternak, E. O. Liedera, and R. M. Liederb, Acta Phys. Pol. B **40**, 647 (2009).

[50] S. Kumar, R. Palit, H. C. Jain, I. Mazumdar, P. K. Joshi, S. Roy, A. Y. Deo, Z. Naik, S. S. Malik, and A. K. Jain, Phys. Rev. C **76**, 014306 (2007).

[51] S. Bhowal *et al.*, Phys. Rev. C **84**, 024313 (2011).

[52] M. Sugawara *et al.*, Eur. Phys. J. A **1**, 123 (1998).

[53] W. Nazarewicz, J. Dudek, R. Bengtsson, T. Bengtsson, and I. Ragnarsson, Nucl. Phys. A **435**, 397 (1985).

[54] W. Nazarewicz, M. A. Riley, and J. D. Garrett, Nucl. Phys. A **512**, 61 (1990).